Sodium Nitrate Flooding Concentrations on the Petrographic and Geomechanical Properties of Sandstone Reservoir Rocks

E. Peretomode[1], A. Hart[2], O. E. Esi[3], O. V. Peretomode[4], R. O. Afolabi[5*]

[1]Department of Petroleum Engineering, Faculty of Engineering, Delta State University, Abraka, Nigeria
[2]Department of Chemical and Biological Engineering, The University of Sheffield, SI 3JD, UK,
[3]Department of Physics, Dennis Osadebay University, Asaba, Delta State, Nigeria, 4Department of Science Laboratory Technology, Delta State University, Abraka, Nigeria.
[4]Department of Science Laboratory Technology, Delta State University, Abraka, Nigeria.
[5]School of Engineering, Robert Gordon University, Aberdeen, AB10 7GJ, UK,

ABSTRACT: The geochemistry and geomechanical characteristics of the reservoir formation can be negatively impacted by fluid flow and fluid-rock interactions. Chemical-rock interaction in the oilfield happens during water injection, chemical flooding, and inhibitor use; the degree of interaction varies with concentration and could impact the rock's petrographic and geomechanical properties. Sodium nitrate ($NaNO_3$) is used to modulate reservoir souring caused by sulphate-reducing bacteria (SRB) during waterflooding. This study investigates how $NaNO_3$ alters sandstone properties at 637.5, 850, 1062.4, and 1275 ppm via core flooding, using Uniaxial Compressive Strength (UCS), Particle Size Distribution (PSD), Scanning Electron Microscopy (SEM) with Energy-Dispersive X-ray spectroscopy (EDX), and X-Ray Powder Diffraction (XRPD) analyses to assess nitrate flooding effects. The findings showed that at sodium nitrate concentrations less than 850 ppm, only minor changes in PSD appeared, whereas at higher concentrations, the particle size distribution changed significantly. Furthermore, SEM/EDX and XRPD results indicated elemental and mineralogical changes, suggesting that the rock-$NaNO_3$ interactions resulted in the dissolution and precipitation of minerals as well as phase transformation. As the sodium nitrate concentration increased from 850 ppm to 1062.4 ppm, the sandstone's permeability and porosity increased significantly from 69±1.2 mD and 12±2.4% to 81±0.4 mD and 20±8% mD, respectively. Thus, at higher $NaNO_3$ concentrations (> 850 ppm), a significant reduction of the UCS of sandstone was observed. Overall, these findings highlight the significant risk posed by higher concentrations of sodium nitrate under dynamic conditions in oilfields, underscoring the need for optimized chemical formulation to prevent reservoir formation damage and operational challenges.

Keywords: Coreflooding, Sandstone, Chemical-rock interaction, Permeability and porosity changes, Rock strength, oilfield chemical

[Received Jan. 24, 2025; Revised Feb 26, 2025; Accepted Dec 14, 2025] Print ISSN: 0189-9546 | Online ISSN: 2437-2110

I. INTRODUCTION

Oilfield chemicals are widely used for enhanced oil recovery (e.g., alkaline, surfactant, and polymer flooding), drilling fluids, and reservoir treatment fluids such as scale inhibitors, scavengers, stimulants, and demulsifiers. Research shows that these chemicals can damage petrophysical and mechanical properties when they interact with reservoir formations. Chemical-rock interactions may cause mineral dissolution or precipitation, which alters the rock's mineralogical, petrophysical, and geomechanical characteristics (Li & Aubertin, 2003; Yang et al., 2017; Wuyep et al., 2018; Alexey, 2022; Mihrin et al., 2022; Halim et al., 2022; Farajollahi et al., 2022). To evaluate geological CO_2 sequestration, the impact of carbon dioxide (CO_2)-NaCl solution on compressive strength and deformation of quartz-feldspar-detrital reservoir sandstone was studied (Zheng, Feng, and Pan, 2015).

It was discovered that CO_2 dissolved in pore fluid lowered sandstone compressive strength by 7-15% when compared to CO_2-free control. This reduction results from precipitation and mineral dissolution reactions driven by chemical-rock interactions, which change the rock's elemental composition, mineralogy, particle size distribution, and porosity. Consequently, reservoir formation interactions with biocides or corrosion inhibitors used to control hydrogen sulphide (H_2S) souring—caused by sulphate-reducing bacteria (SRB)—can also alter petrophysical and geomechanical properties (Wuyep et al., 2018; Peretomode et al., 2025). Due to the environmental hazards of biocides and inhibitors for H_2S control, a technology using nitrates for reservoir souring treatment, called biocompetitive exclusion (BCX), has been adopted (Hurbert, 2010). Laboratory studies have examined nitrate use for reservoir souring control and enhanced oil recovery (Reinsel et al., 1996; Telang et al., 1998; Sunde et al., 2004; Greene et al., 2006; Grigoryan et al., 2008; Hubert, 2010; Voordouw et al., 2011; Tabari et al., 2011; Hitzman & Sperl, 1994; Sandbeck & Hitzman, 1995; Giangiacomo & Dennis, 1997; Zhao et al., 2016). Previous research on nitrate-reservoir rock interactions has focused mainly on static conditions for microbial treatment. For instance, Peretomode et al. (2025) studied the effect of nitrate on the petrophysical and mechanical properties of sandstone reservoir

Corresponding author: peretomodee@delsu.edu.ng
*doi:*http://.doi.org/10.63746/njtd.v22i5.3320

rock under static saturation, which is governed only by diffusion and simulates shut-in conditions during reservoir treatment. While these studies provide valuable insights, the effects of nitrate influx on geochemical and geomechanical properties during dynamic conditions remain unexplored. To address this, dynamic coreflooding study will be explored here to mimic chemical injection operations followed by reservoir production in the industry.

Dynamic coreflooding, governed by diffusion and convection, allows assessment of reactive fluid movement through the rock porous matrix. Building on the distinction between static and dynamic conditions, flooding reactive fluids through heterogeneous rocks and dissolving specific mineral phases is common in reservoirs. The heterogeneous porous structure reveals the natural variability of reservoir rocks (Min et al., 2016). The degree of mineral alteration, which results from dissolution and precipitation reactions during chemical-rock interactions, depends on several factors. These include concentration, pH, reservoir type, fluid flow rate, temperature, and rock mineralogical composition (Peretomode et al., 2022; Peretomode et al., 2024; Peretomode et al., 2025). On the other hand, reservoir parameters such as permeability and porosity and rock strength are especially prone to adverse geomechanical effects. Understanding these processes is essential for evaluating reservoir formation behavior and the risk of sand production linked to chemical-rock interactions under dynamic conditions. This research aims to systematically evaluate the effects of sodium nitrate (NIT) on elemental and mineralogical composition, porosity, permeability, particle size distribution, uniaxial compressive strength (UCS), and Young's modulus of sandstone reservoir rock under dynamic conditions. The primary objective is to identify optimal nitrate concentrations for effective biocompetitive exclusion (BCX) treatment that controls reservoir souring while maintaining formation integrity. Additionally, the study will quantify impacts on rock properties to assess whether BCX treatment offers a viable solution for reservoir management.

II. MATERIALS AND METHODOLOGY

The chemical salt properties are listed in Table 1. Deionized water prepared brine solutions simulating reservoir conditions. Eighteen identical Leopard sandstone core samples (Kocurek Industries) with an L/D ratio of 2.0 (ASTM standard) were utilized. Tests were repeated four times per concentration for reliability. Uniaxial compression tests determined rock strength before and after sodium nitrate flooding. Post-flooding, samples were analyzed using SEM/EDX and XRPD to examine morphological and mineralogical changes. Particle size distribution of effluents was measured via laser diffraction. Permeability was determined via Darcy's law, and porosity was measured using an ICP-OES lithium tracer method. Core-flooding experiments were conducted using a custom-built rig.

A. Materials

The properties of the chemical salts used in this study are presented in Table 1. The concentrations are similar to that reported in the literature by Oluyemi (2014). The deionized water was used to prepare brine solutions to simulate brine conditions within reservoir formation.

Eighteen (18) identical Leopard sandstone core samples (Kocurek Industries, Inc. in Texas, USA) with a L/D ratio of 2.0 according to the ASTM standard were used for this test. The test was repeated four (4) times for each sample concentration for reliability. Table 2 shows the geometrical parameters for the coreflooding test.

Table 1 Brine composition in a 500ml deionised water

Salts	**Active ions**	**Concentration (PPM)**
NaCl	Na^+	10392
$CaCl_2 2.H_2O$	Ca^{2+}	426
$MgCl_2.6H_2O$	Mg^{2+}	630
KCl	K^+	208
$SrCl.6H_2O$	Sr^{2+}	10

Table 2 Geometrical parameters for coreflooding experiment.

Parameters	**Sandstone**
Length (mm)	102
Diameter (mm)	51
L/D	2.0
Porosity (%)	20-22
Permeability (mD)	1100-1300

B. Uniaxial Compression Test

The strength of the rock was determined before and after sodium nitrate flooding using length-to-diameter ratio correction factors. The treated samples were oven-dried and subjected to uniaxial compression tests using mechanical equipment as reported in the literature (Kohmura & Inada, 2006; Sun, et al., 2012; Fabjan, et al., 2015). The core samples' UCS was measured and recorded before and after static and dynamic flooding tests, using a built-in data logger and Young's modulus plot.

C. Analytical Test

The changes in the sandstone core, due to sodium nitrate dynamic flooding were examined. The core samples were prepared for analytical tests by drying, grounding, and degreasing. The Scanning Electron Microscopy (SEM) integrated with Energy-Dispersive X-ray spectroscopy (EDX) (SEM/EDX) test provided high-resolution images of minor features and morphological changes in core samples, allowing the examination of authigenic clays and cement. X-ray powder diffraction (XRPD) was used to identify phase change due to nitrate-rock interactions and examine mineral phases in untreated

and treated samples using Panalytical X'Pert powder X-ray diffractometer based on protocol reported elsewhere (Wuyep et al., 2018). The rock samples were wet grounded in ethanol and spray-dried, with cobalt radiation recorded. Quantitative analysis was performed to determine the mineralogical composition of the rock samples using Malvern Panalytical suits.

D. Particle Size Distribution Test

The Malvern Laser Mastersizer 3000E was used to measure the particle size distribution (PSD) for both static and dynamic flooding effluents. To ensure accuracy, the system was rinsed with deionized water, drained, and repeated thrice with clean water. The PSD was measured in weight percent, and the effluent sample is dropped into the continuously stirred water.

E. Permeability Measurement

The permeability analysis was carried out by sequentially passing brine through the core sample at varying rates of 2, 4, 3, and 2 mL/min based on methodology reported in the literature (Wuyep, 2018). Flow rate and differential pressure data collected through LabView. The collected data was used to determine the permeability of the core samples using Equations 1 and 2.

Before measurement, the core holder and injection lines were tested for pressure leakages. Thereafter, its permeability was determined by pumping 2 mL/min of brine through the mounted core sample. The differential pressure of fluid flow from the pump to the core holder, was sensed by the National Instruments data acquisition system (NIDAQ) and recorded on the Laboratory Virtual Instrument Engineering Workbench (LabView), which was measured using a Validyne CD223 pressure transducer. The core's permeability before and after chemical saturation was calculated based on Darcy's law (Equation 1), which utilizes the measured pressure drop across the core, since the viscosity of the fluid and size of the core samples are known.

$$Q = \frac{KA}{\mu}\frac{dP}{dL} \dots\dots\dots\dots\dots\dots\dots\dots\dots\dots\dots\dots\dots\dots\dots\dots (1)$$

$$From\ the\ above\ equation, K = \frac{Q\mu L}{A.\Delta P} \dots\dots\dots\dots (2)$$

Where Q denotes the flow rate (cm^3/sec), K the permeability (D), μ the fluid viscosity (cP), and $\frac{dP}{dL}$ the differential pressure per unit length (atm). Once the pressure differential of the flow across the sample's core has been determined, its permeability can be calculated using Equation 2. Thus, the permeability of the sample before and after treatment with Sodium Nitrate was compared to assess changes in permeability.

F. Measurement Using ICP-OES Analysis

The core's porosity was determined both before and after the injection of sodium nitrate. The porosity was determined using Inductively Coupled Plasma Optical Emission Spectroscopy (ICP-OES) analysis of lithium tracer gathered from the sample's effluents. This technique was used because it is inert, does not interfere with the reaction, and it is widely used by researchers (Jordan, et al., 1994; Oluyemi, 2014; Wuyep, et al., 2018).

A lithium tracer from a stock of 10,000 ppm standard was made by diluting 2.0 ppm lithium in deionized water to determine the flooding test core's porosity. The prepared Lithium tracer (500 ml) was calibrated with deionized water and analyzed following the standard shown in Figure 1. Although the sample's pore volume was predicted to be 25 ml using the liquid saturation method, 40 ml of the prepared 500 ml lithium tracer was injected into the core at a constant flow rate of 2 mL/min. The effluent was collected and examined with ICP-OES every five minutes. This process was repeated first for brine and then for nitrate flooding at varying concentrations of 637.5 ppm, 850 ppm, 1062.4 ppm, and 1275 ppm. These concentrations were based on early research work published in the literature (Hubert & Voordouw, 2007; Peretomode et al., 2025).

The normalized concentration values (C/Ch) were plotted against the cumulative volume. The Li tracer procedure was repeated after every chemical injection. The dead volume, pore volume, bulk volume, and porosity were calculated from the Li tracer profile data generated. Equation 3 was used to determine the porosity (∅). Whereas Equations 4 and 5 were used to determine the core sample's pore volume V_p, total volume V_T, and dead volume V_d, respectively.

$$\emptyset = \frac{V_p}{V_b} \times 100\% \dots\dots\dots\dots\dots\dots\dots\dots\dots\dots\dots\dots\dots\dots\dots (3)$$

V_p denotess the pore volume and V_b the bulk volume of the core sample.

$$V_p = V_T - V_d \dots\dots\dots\dots\dots\dots\dots\dots\dots\dots\dots\dots\dots\dots\dots (4)$$

Where the total volume V_T is the summation of the product of the normalized concentration and the sample volume as shown in Equation 5.

$$V_T = \sum\left(\frac{C}{C_h} \times Sv\right) \dots\dots\dots\dots\dots\dots\dots\dots\dots\dots\dots\dots\dots\dots (5)$$

Where S_v represents the sample volume.

The dead volume V_d is the summation of the lengths of the tubes from the pump to the core holder (inlet) and outside the core holder (outlet) (Equation 6).

$$V_d = \pi r^2 L\ of\ inlet + \pi r^2 L\ of\ outlet \dots\dots\dots\dots (6)$$

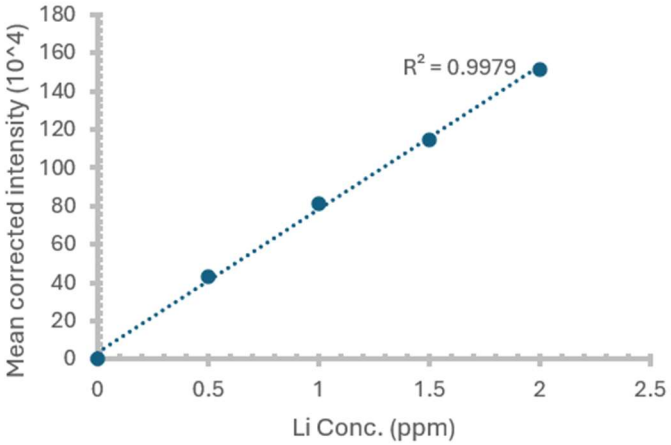

Figure 1. Lithium tracer profile.

G. Core-Flooding Experiment

The experimental coreflooding rig was designed and constructed at the Robert Gordon University (RGU), UK. The coreflooding system consists of a 220V injection pump, used to supply injection fluid into the test core sample. The operating range of the pump is as follows: flow rate (0.1-12.00 ml/min) and pressure (0-6000 psi), with reliability within ±2%. Figure 2 shows the schematic diagram of the coreflooding process used in this study. The core flooding (convection and diffusion) was significant in accounting for the effect of fluid flow, thereby mimicking field operations and production from the reservoir rock.

The core sample was saturated for six hours at ambient temperature, then sodium nitrate was introduced at a rate of 0.25 mL/min until full saturation, with various injection concentrations shown in Table 3. This flow rate was used in order to prevent swift pressure surges and turbulent flow, which resulted from a higher flow rate. Consequently, the core flooding system has been optimized for 0.25 mL/min, which has been published elsewhere (Wuyep et al, 2020). Also, the concentrations were consistent with static effect study of sodium nitrate on sandstone reservoir published elsewhere (Peretomode et al., 2025).

A high-performance syringe pump (HPLC 1500), powered by 220 V, injects NIT into the core at a flow rate of 0.25 mL/min. The NIT is then left to interact with the core sample for 24 hours, after which brine is injected into the sample core to flush out the NIT. 0.25 mL/min is the rate at which NIT was flushed out of the core to avoid any particle release due to flow rate effects (Ochi & Vernoux, 1998; Oliveira, et al., 2014; Wuyep, et al., 2020). A low-capacity 0-12.5 Validyne differential pressure transducer linked to a PC equipped with a Laboratory Virtual Instrument Engineering Workbench (LabVIEW) programme for data logging and monitoring. The differential pressure of the inlet and outflow over time was recorded using a National Instruments data acquisition system (NIDAQ) as shown in Figure 2. A detailed description of the coreflooding experimental protocol has been reported elsewhere (Peretomode et al., 2025).

Table 3 Different Nitrate concentrations in 200 ml (Hubert & Voordouw, 2007)

Compound	Concentration (ppm)
Nitrate (sodium Nitrate)	637.5
	850
	1062.4
	1275

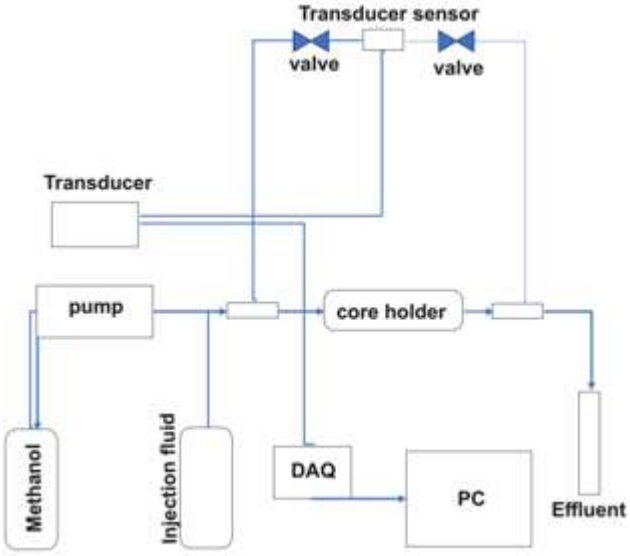

Figure 2: Schematic diagram for core flooding.

III. RESULTS AND DISCUSSIONS

A. Concentration Effect on Elemental and Mineralogical Composition.

Quartz is the main mineral component in sandstone. Hence, the rock-$NaNO_3$ interaction during the dynamic flooding is likely to result in the chemical reaction shown in Equation 7.

$$2NaNO_3 + SiO_3 \rightarrow Na_2SiO_2 + N_2O_5 \quad (7)$$

This shows the pathway for silica dissolution in sandstone and weakens the cement within the rock (Abes and Andreas, 2024; Peretomode et al., 2024). SEM photomicrographs in Figures 3a–f show core sample morphologies: (i) untreated, (ii) brine-treated, and (iii–vi) sodium nitrate-treated sandstones at 637.5, 850, 1062.4, and 1275 ppm. The corresponding EDX reveals the elemental composition for each condition.

Figure 1. SEM photomicrographs at 20 μm scale for (a) untreated sandstone (b) brine treated (c) 637.5 ppm (d) 850 ppm (e)1062.4 ppm and (f) 1275 ppm.

The SEM images reveal pitting or indentations on the rock particles. These features confirm grain particle detachment and mineral alterations due to dissolution or precipitation from chemical-rock interactions. Specifically, the interaction of sodium nitrate with sandstone weakens the silicon-oxygen bonds on the surfaces of quartz and silicate minerals, resulting in dissolution (Peretomode et al., 2024). As the chemical concentration increases, the proportion of indentations or pits observed on the rock particle surfaces becomes more evident and pronounced. For example, the 1275 ppm $NaNO_3$ treated sample shows greater pitting compared to the 637.5 ppm sample. Consequently, under dynamic conditions, sodium nitrate concentration plays a critical role in controlling silica dissolution, which is crucial for maintaining formation strength and mitigating sand production risks. Table 4 displays the mineral

changes and elemental composition of samples subjected to various sodium nitrate concentrations.

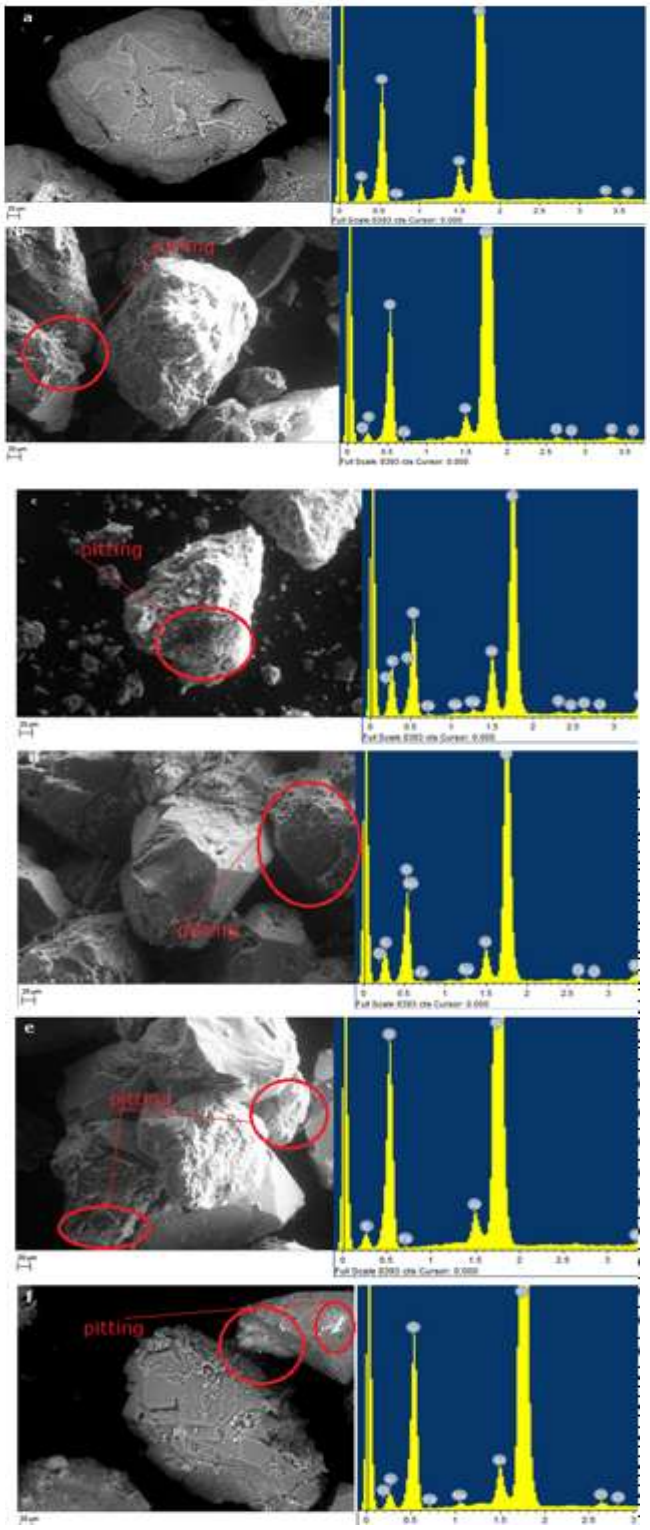

Figure 3. SEM photomicrographs at 20 µm scale for (a) untreated sandstone (b) brine treated (c) 637.5 ppm (d) 850 ppm (e)1062.4 ppm and (f) 1275 ppm.

Table 4. Elemental composition of sandstone rock pre- and post-chemical flooding.

Elements	Untreated (wt.%)	Brine (wt.%)	1275 PPM (wt.%)	1062.4 PPM (wt.%)	850 PPM (wt.%)	637.5 PPM (wt.%)
O	50.16	50.37	48.87	50.41	49.33	47.27
Al	3.51	2.56	2.48	4.08	4.08	7.97
Si	43.9	44.78	45.50	42.02	41.78	32.90
K	0.89	0.69	0.52	0.79	0.89	2.41
Fe	1.30	1.19	1.37	2.17	2.45	6.86
Mg	0.07	0.08	ND	0.11	0.12	0.55
Cl	0.05	0.23	0.52	0.22	0.25	0.78
Ti	0.12	0.06	ND	0.05	0.39	0.25
Ca	ND	0.04	ND	0.05	ND	0.39
Na	ND	ND	0.31	0.05	0.12	0.45
Mn	ND	ND	0.43	ND	0.46	ND

The EDX shows significant silica (Si and O) for both untreated and chemically treated sandstone cores. This is because a sandstone reservoir formation is a siliciclastic sedimentary rock. It is comprised of sand grains (i.e., silica) and other minerals that act as binding materials. These minerals are found between the particles within the formation. This observation provides insight into the likelihood of a decrease in rock strength. Such weakening results from mineral dissolution and precipitation during interactions between injected sodium nitrate/brine and sandstone, especially quartz. Dissolution starts with clay swelling, carbonate dissolving, and hydrolysis of silicate minerals. These minerals contain Si-O-Si or Si-O-M bridges, where M is a metal ion. As a result, clay mineral alteration and changes in dispersion can affect rock permeability and porosity. These effects can either increase or decrease these properties. The clay material, therefore, strongly impacts formation integrity (Yustiningtyas, 2012). The clay phase in sandstone may react at a rate different from that of silica depending on the $NaNO_3$ concentration. Thus, the dissolution rate along grain boundaries influences detachment from the rock surface, depending on concentration. Grain boundaries respond at different rates according to the mineral phase present (Israeli & Emmanuel, 2018). Notably, at 637.5 ppm of $NaNO_3$, there is a significant reduction in the Si amount due to mineral dissolution. This is revealed by observed pitting on the SEM image (Figure 3c). On the other hand, amounts of Fe, Cl, and Mg increased after chemical treatment. This signifies a precipitation reaction because of rock-$NaNO_3$ interactions. This finding matches the pitting seen on SEM images of chemically treated samples, unlike untreated samples.

Figures 4a–f shows the XRPD patterns at 20 m and mineral changes in brine-treated sandstone, relative to the untreated sample at 637.5 ppm, 850 ppm, 1062.4 ppm, and 1275 ppm sodium nitrate. In the untreated sample, peaks at 2θ = 21°, 26.5°, 40.5°, and 50° represent quartz, making up about 47% of the sample, while clay minerals such as kaolinite are present with peaks at 2θ = 12.3°, 22°, and 38.5°. Furthermore, biotite minerals (about 16%) appear in the XRPD pattern (Figure 5a). In contrast, wollastonite, a calcium inosilicate mineral ($CaSiO_3$) that may include trace elements such as iron, magnesium, and manganese, can be observed in the brine-treated sample. Another mineral, ferrierite-Mg, with a composition similar to zeolite, can also be observed in the XRPD pattern. Thus, quartz hydrolysis and dissolution resulting from sodium nitrate-sandstone reactions could lead to sand production, depending on sodium nitrate concentration (Alameen et al., 2024). These observations suggest high likelihood of changes in porosity, permeability, and particle size distribution as the concentration of the $NaNO_3$ increases due to dissolution and precipitation reactions. These findings emphasize the key role of cementitious materials in maintaining sandstone reservoir integrity, as their weakening and detachment would lead to formation damage and sanding.

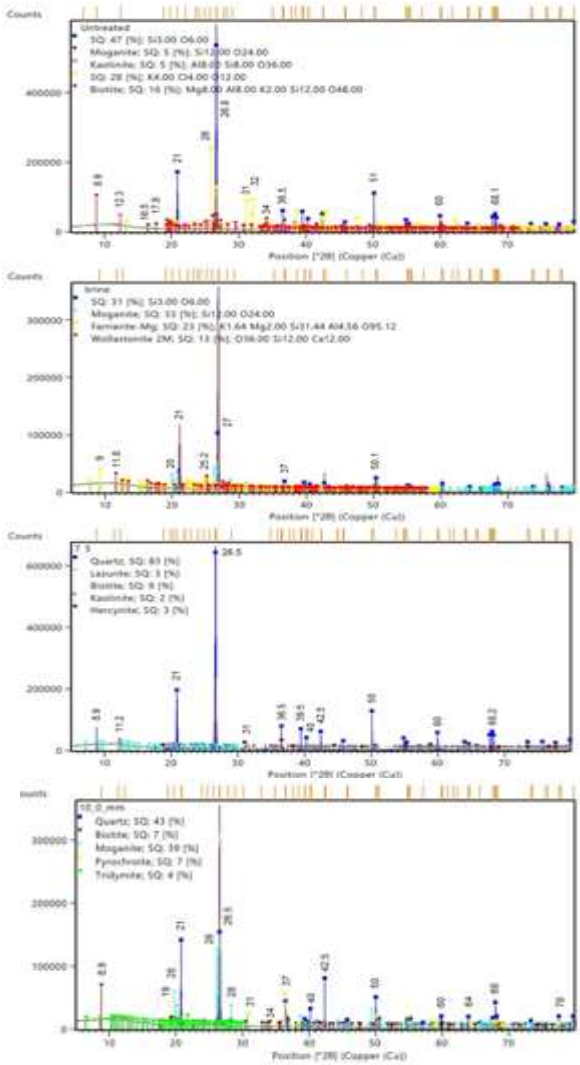

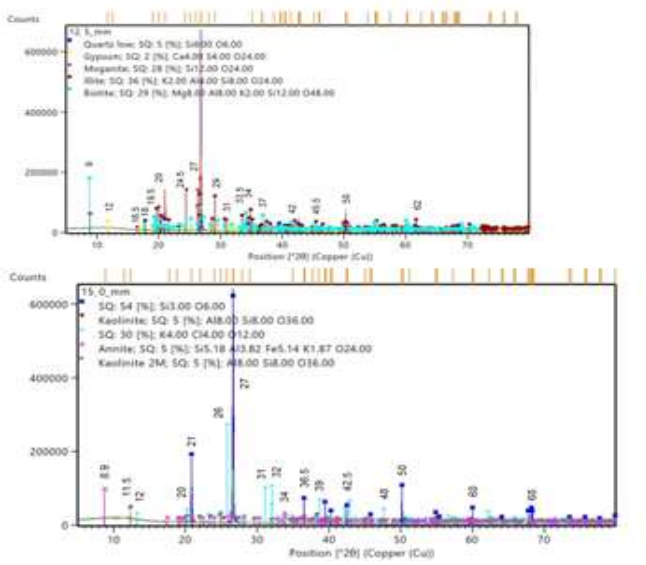

Figure 2. XRPD mineralogy and clay composition for (a) untreated sandstone, (b) brine treated, (c) 637.5 ppm, (d) 850 ppm, (e) 1062.4 ppm, and (f) 1275 ppm.

The results show that a $NaNO_3$ concentration of 637.5 ppm causes more precipitation of quartz, approximately 83%. This is indicated by the high peak intensity at 2θ = 21° and 26.5°. Due to the dissolution and precipitation of minerals from interactions between $NaNO_3$ and rock, the untreated sample allows for the identification of lazurite and hercynite. Interestingly, moganite peak intensities are higher in the sample subjected to 850 ppm $NaNO_3$. This is due to silica precipitation following quartz dissolution. The decrease in the peak intensity of quartz confirms its dissolution when the $NaNO_3$ concentration increased to 850 ppm. This affirms that the rate of chemical reactions increases as the concentration of $NaNO_3$ increases. The quartz component of the sample treated with 1062.4 ppm $NaNO_3$ is much lower than the quartz component of the brine-treated sample. This suggests that the concentration of $NaNO_3$ has a notable impact on the quartz component of rock formation. This is consistent with the pitting observed on SEM images of the core samples in Figures 4a-f. Conversely, the precipitation of a clay mineral, illite, is observed on the XRPD pattern of the sample treated with 1062.4 ppm $NaNO_3$. When the sample was treated with 1275 ppm $NaNO_3$, the formation of annite occurred. Annite is an iron end member of the mineral biotite. This indicates that annite is a precipitate of dissolved biotite.

The results confirm changes in sandstone mineralogy and morphology due to the interaction of the BCX chemical, sodium nitrate flooding. These changes increase as sodium nitrate concentration rises, clearly demonstrating a consequential impact on the rock's permeability, porosity, particle size distribution (PSD), Unconfined Compressive Strength (UCS), and Young's modulus. This aligns with past research where injected chemical concentrations induced deformation in the rock by changes in the rocks petrophysical properties (Shellis et al., 2010; Lins et al., 2013; Sanda & Taiwo, 2016).. The outcome of chemical deterioration and rock particle detachment corroborate with

earlier published studies (Kahraman, et al., 2008; Wuyep, et al., 2020).

B. Effect of Chemical Concentration on Particle Size Distribution

Figure 5 shows PSD patterns under flooding at the various concentrations investigated. While the changes in the PSD D_{10}, D_{50}, and D_{90} determined using the Malvern Mastersizer 3000M are shown in Table 5. It can be observed that there are changes in PSD for the original brine, brine uptake, and particles flooded with sodium nitrate at concentrations of 637.5 ppm, 850, 1062.4, and 1275 ppm. Notably, PSD profiles for flooding with sodium nitrate concentrations of 637.5 and 850 ppm show a similar pattern. Likewise, the original brine and brine uptake are identical, while the trend profiles of sodium nitrate concentrations of 1062.4 ppm and 1275 ppm are identical (Figure 5). These similarities are evident in their respective particle sizes, D10, D50, and D90, as shown in Table 5. Although a slight change in the PSD of brine effluent compared to the original brine is observed for D50 and D90, there is no indication that the rock's grain fabric has been damaged physically or chemically by brine-rock interactions. On the other hand, only a slight change in D50 from 72 to 80 µm is observed for 637.5 ppm and 850 ppm concentrations of nitrate flooding. This small increase in D50 indicates a minor chemical effect caused by the fluid-rock interactions, likely resulting from the dissolution process. Therefore, sodium nitrate at concentrations of 637.6 ppm and 850 ppm does not significantly impact the particle size distribution through chemical reactions. In contrast, substantial changes in particle size are observed at higher concentrations of 1062.4 ppm and 1275 ppm. These larger changes imply that, at higher nitrate concentrations, chemical interactions between the fluid and rock cause significant detachment of grain particles from the core matrix, which are then flushed out with the brine. Thus, fluid-rock interactions at concentrations above 850 ppm can lead to particle detachment, plausible formation damage and sanding. The released grain particles are expected to influence the rock's porosity, permeability, and strength.

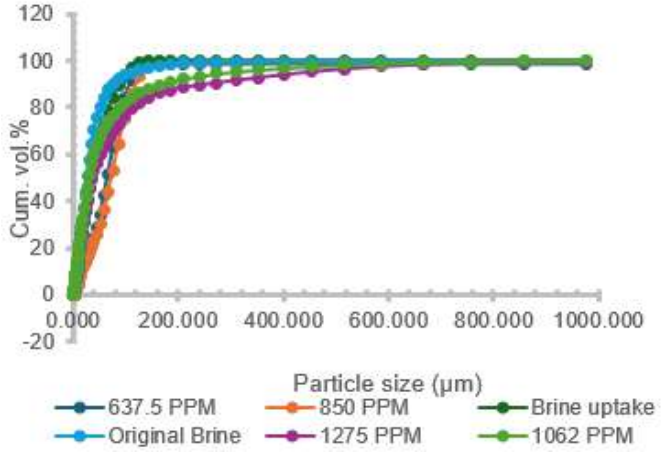

Figure 5 Grain size distribution profile for brine, 637.5 ppm, 850 ppm, 1062.4 ppm, and 1275 ppm sodium nitrate concentration flooded sandstone core.

Table 5 D10, D50 and D90 for original brine, brine uptake, 637.5 PPM, 850 PPM, 1062.4 PPM and 1275 PPM under flooding

Parameters	D_{10} (µm)	D_{50} (µm)	D_{90} (µm)
Original Brine	10	36	80
Brine Uptake	10	40	82
637.5 PPM	20	72	118
850 PPM	20	80	120
1062.4 PPM	10	40	160
1275 PPM	10	40	220

C. Concentration effect on porosity and permeability

The changes in mineralogical and observed pitting on the SEM reinforced silica dissolution following sandstone-$NaNO_3$ interactions (Figures 4-6), can potentially alter the permeability and porosity of the rock, thereby reducing formation strength (Alameen et al., 2024). The lithium tracer profile, which was used to calculate the porosity of the sandstone core samples is shown in Figure 7. The lithium tracer effluent was produced by flooding the core with brine and sodium nitrate at concentrations of 1275, 1062.4, 850 and 637.5 ppm, respectively. The mean porosities obtained after flooding the rock core with brine and sodium nitrate concentrations of 637.5 and 850 ppm, respectively, are 11±0.8%, 11±1.8%, and 12±2.4%. From Figure 6, it can be observed that the cumulative volume (mL) (20) at 1062.4 ppm is higher when compared to the volume at 1275 ppm concentration.This may be due to the pore size volume. The similarity of porosity for sodium nitrate concentrations at 637.5 and 850 ppm is consistent with the PSD profiles of both reported in Figure 6. The results for the brine, 637.5 and 850 ppm concentrations of $NaNO_3$ appear to agree with the visual observations of detached particles. Correspondingly, no significant changes in rock permeability 68±4.3 mD, 69±0.6 mD, and 69±1.2 mD were noticed for the same chemicals and concentrations.

As the concentration of sodium nitrate was increased to 1062.4 and 1275 ppm, the mean porosity of the rock core increased to 20±8% and 21±5%, respectively, following flooding. Likewise, significant changes were observed in the rock's permeability, which are 81±0.4 mD and 84±6 mD for 1062.4 ppm and 1275 ppm treatments, respectively. The increased porosity with a corresponding rise in permeability indicates a well-structured pore network because of the rock's pore space connectivity. As a result, a concentration of sodium nitrate greater than 850 ppm can trigger significant chemical reactions capable of modifying the microstructure of sandstone reservoir, such as grain detachment and pore size alterations. Thus, sodium nitrate's interaction with rock samples is concentration dependent. This suggests that more rock particles may have dissolved or that the minerals in clay may have undergone a transformation (Torok & Vasarhelyi, 2010; Wuyep, et al., 2018; Irwan, 2021)

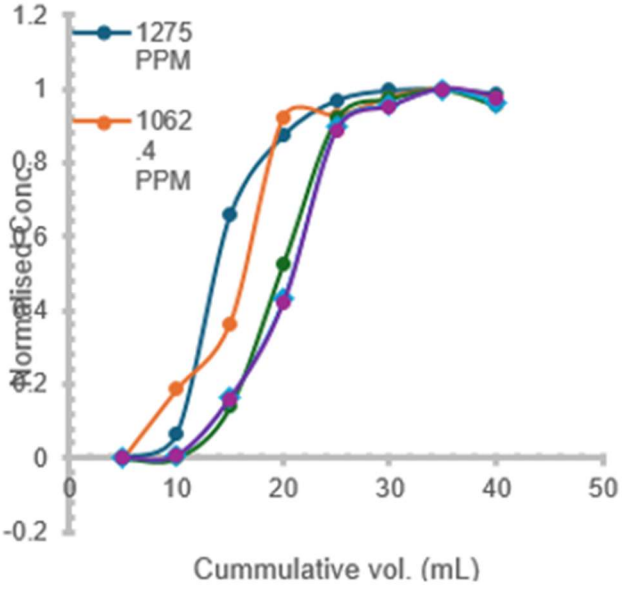

Figure 6. Lithium tracer profile for initial flooding, 637.5 ppm, 850 ppm, 1062.4 ppm and 1275 ppm sodium nitrate concentration flooding

D. Concentration Effect on UCS And Young's Modulus

The stress-strain profiles of the untreated and sodium nitrate-treated samples are displayed in Figures 7a and b, respectively, at concentrations of 637.5, 850, 1062.4, and 1275 ppm. It is evident that the UCS of the untreated and brine-treated samples decreased from 34±0.7 MPa to 29±0.4 MPa. This represents 14.7% decrease in the strength of the sandstone core sample, which corroborates with the negligible effect of brine-rock interaction on porosity and particle size distribution. However, after treatment with sodium nitrate at concentrations of 637.5, 850, 1062.4, and 1275 ppm, the mean UCS of the Leopard sandstone samples decreased from 29±0.4 MPa (brine-treated) to 23±0.1 MPa, 18±4 MPa, 17±2 MPa, and 14±0.9 MPa, respectively. The error bars represent standard deviations of triplicate experiments and indicate variation from the mean values in the range of ±0.1 to ±4. This is less than 1%, showing good reproducibility of the data. This implies a UCS decrease in the range of 32.35 to 58.82% as $NaNO_3$ concentration increased from 637.5 to 1275 ppm relative to the untreated sandstone core sample. Compared with the static saturation study reported by Peretomode et al. (2025), where UCS dropped by 5% (brine-treated) and 9% for $NaNO_3$ treated. As a result, under dynamic flooding, the $NaNO_3$-sandstone interaction has a greater impact on the rock's petrographic and geomechanical properties than static saturation. As shown earlier, the decreased UCS with increasing sodium nitrate concentration is consistent with increased porosity due to higher chemical reactions, such as dissolution and precipitation reported in section 3.3. As the $NaNO_3$ concentration increased from 850 to 1062.4 ppm, a significant change can be observed in the porosity and UCS relative to the untreated sandstone core. Hence, at a concentration greater than 850 ppm, the $NaNO_3$-sandstone interaction during dynamic flooding induces considerable dissolution and sand grain detachment, reducing core strength and potentially causing formation damage and sanding. The changes in UCS observed in this study due to sodium nitrate concentration increase from 637.5 to 1275 ppm, agrees with previous research where varying concentrations of NaCl brines and rock induced failure upon interaction (Shukia, et al., 2013). The trend is consistent with the result shown in Figure 6.As demonstrated in section 3.3 of this study, the dissolution of the rock's bonding minerals may be connected to the decrease in the rock's UCS, increasing porosity and permeability (Alameen et al., 2025). It is, however, worth noting that the measured UCS of the untreated sample (34±0.7 MPa) is outside the specified UCS of 21–26 MPa of the Kocurek Industries Ltd. Consequently, the results of this investigation are analogous to earlier studies that examined how chemical fluid interaction affects the porosity, permeability, and mechanical strength of rocks (Baba, et al., 2005; Safari, et al., 2009; Sanda & Taiwo, 2016).

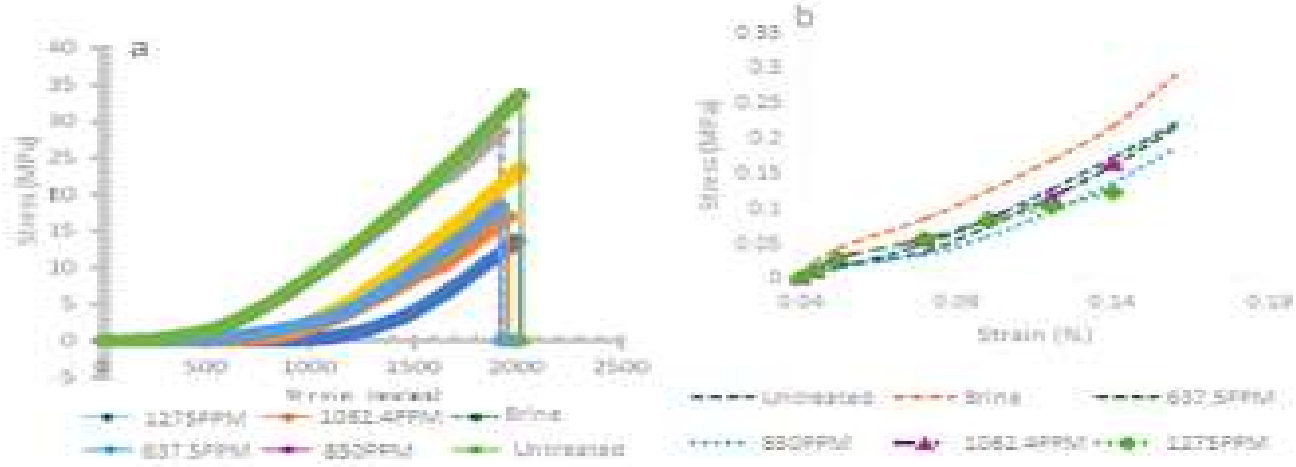

Figure 7. untreated, 637.5 PPM, 850 PPM, 1062.4 PPM and 1275 PPM NaNO3 treated sandstone for (a) UCS and (b) Young's modulus.

Young's modulus mechanically gauges rock rigidity under tensile or compressive loads. Figure 7b displays the rock samples' Young's modulus as a function of sodium nitrate concentration. The results of the untreated rock sample, the brine-treated, and the samples treated with 637.5 and 850 ppm sodium nitrate concentrations are as follows: 216±4.8 MPa, 199±3.2 MPa, 170±2.4 MPa, and 196±2.1 MPa (Table 6), respectively. However, when the samples were flooded with NaNO3, Young's modulus decreased by 46 MPa (637.5 ppm) and 20 MPa (850 ppm) relative to the untreated sample (216±4.8 MPa). Notably, the highest standard deviation (±4.8) of triplicate experiments is less than 1%, indicating good reproducibility of the results. But when the NaNO3 concentration was increased to 1062.4 ppm and 1275 ppm, the Young's modulus of the treated samples decreased to 196±0.2 MPa and 106±0.9 MPa, respectively (Table 6). This represents a decrease of approximately 9% and 51% in Young's modulus relative to the untreated sample (216±4.8 MPa), which can be attributed to alterations in microstructure resulting from fluid-rock interactions. The Young's modulus of both the 850 ppm and 1062.4 ppm nitrate-treated rock samples was the same, proving that both concentrations, on interaction with the rock, had the same impact on the rock's modulus. It has previously been demonstrated that sodium nitrate interaction with rock samples resulted in substantial changes in microstructure, such as increased pore size and permeability compared to brine. This explains why sodium nitrate has a more significant effect on the Young's modulus of the rock. Although the test conditions are different, the impact of sodium nitrate on sandstone rock strength is consistent with water saturation, as reported in a previous study (Cai et al., 2019).

The rock UCS characteristic can directly relate to rock porosity, PSD, and elemental and mineral compositions. The results show that the samples flooded with the highest NaNO3 concentration (1275 ppm) have the lowest UCS (14±0.9 MPa). A second-order polynomial model with an R^2 coefficient of 0.961 offered the best fit for the UCS concentration data, as shown in Figure 8. The model validates the experimental findings that, as the concentration of $NaNO_3$ rises, the UCS of the rock samples decreases. Although the second-order polynomial model is empirical, it can predict the UCS from the sodium nitrate concentration with an error of about 4%.

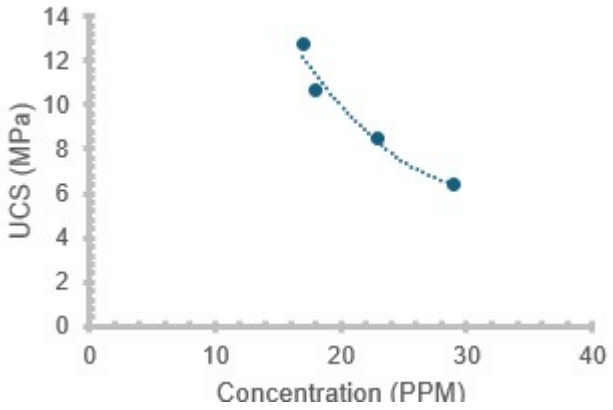

Figure 8. Relationship between concentration and UCS.

IV. CONCLUSION

Chemical-rock interactions are critical in oil and gas production as they have a broad range of impacts including altering rock strength and permeability, contributing to the formation failure and sanding. This study examined how interactions between sodium nitrate and rock occur when flooding sandstone cores with increasing concentrations of sodium nitrate, specifically for controlling reservoir souring and its impact on petrographic and geomechanical characteristics. The results show that sodium nitrate alters elemental composition and mineral phases. Compared to brine-treated samples, sandstone exposed to higher sodium nitrate concentrations shows reduced UCS strength and Young's modulus. As the sodium nitrate concentration increased from 850 ppm to 1062.4 ppm, the sandstone's porosity increased and UCS decreased significantly from 12±2.4% and 18±4 MPa to 20±8% and 17±2 MPa relative to the untreated sandstone core sample, 11±0.8% and 34±0.7 MPa. Thus, at concentrations greater than 850 ppm, the interactions between sodium nitrate and sandstone under dynamic flooding can result in considerable cementitious material dissolution, silica grain detachment and weakening of the grain boundary, and a reduction in geomechanical characteristics. This study demonstrates that during dynamic flooding,

REFERENCES

Abes, A., and M. Andreas (2024). Dynamic-permeability variations induced during CO_2-EOR application in carbonate reservoirs: Upper Red River Formation, North Dakota. *SPE Journal*, 29: 6402–6417. https://doi.org/10.2118/218137-PA.

Alameen, M. B.; A. K. Elraies; A. Almansour; and M. Mohyaldinn (2024). Experimental study of the silica dissolution onto sandstone formation: Influence of pH, salinity, and temperature on dissolution. *Geoenergy Science and Engineering*, 234: 212632. https://doi.org/10.1016/j.geoen.2024.212632.

Alameen, M. B.; A. Almansour; K. A. Elraies; M. Mohyaldinn; and E. Abdulmuez (2025). A novel technique to control sand production from mature consolidated sandstone formation by using sodium phosphate to enhance the formation strength. Paper presented at the *International Petroleum Technology Conference*, Kuala Lumpur, Malaysia, February 2025. https://doi.org/10.2523/IPTC-24777-EA.

Cai, X.; Z. Zhou; K. Liu; X. Du; and H. Zang (2019). Water weakening effects on the mechanical behaviour of different rock types: Phenomena and mechanisms. *Applied Sciences*, 9(20): 4450.

Fabjan, T.; M. D. Ivars; and V. Vukadin (2022). Numerical simulation of intact rock behavior via the continuum and Voronoi tessellation models – A sensitivity analysis. *Acta Geotechnica Slovenica*, 12(2): 5–23.

Farquhar, R. A.; J. M. Somerville; and D. B. G. Smart (1994). Porosity as a geomechanical indicator: An application of core and log data and rock mechanics. SPE, Richardson, Texas.

Halim, M. C.; H. Hamidi; and A. R. Akisanya (2022). Minimizing formation damage in drilling operations: A critical point for optimizing productivity in sandstone reservoirs intercalated with clay. *Energies*, 15: 162. https://doi.org/10.3390/en15010162.

Hill, S. H.; M. C. Villeneuve; and K. N. Bassett (2019). Geomechanical characterization of reservoir rocks in the southern Taranaki Basin, New Zealand. U.S. Rock Mechanics/Geomechanics Symposium, New York, USA.

Hubert, C. (2010). Microbial ecology of oil reservoir souring and its control by nitrate injection. In *Handbook of Hydrocarbon and Lipid Microbiology*. Springer, Berlin, Heidelberg.

Hubert, C., and G. Voordouw (2007). Oil field souring control by nitrate-reducing *Sulfurospirillum* spp. that outcompete sulfate-reducing bacteria for organic electron donors. *Applied and Environmental Microbiology*, 73(8): 2644–2652.

Irwan, A. G. (2021). Effect of porosity on uniaxial compressive strength in sedimentary rocks. *Promine*, 8(2): 61–64.

Israeli, Y., and S. Emmanuel (2018). Impact of grain size and rock composition on simulated rock weathering. *Earth Surface Dynamics*, 6(2): 319–327.

Jordan, M.; K. S. Sorbie; P. Jiang; M. D. Yuan; A. C. Todd; and K. E. Hourston (1994). Phosphonate scale inhibitor adsorption/desorption and the potential for formation damage in reconditioned field core. Society of Petroleum Engineers.

Kahraman, S.; O. Gunaydin; and M. Fener (2008). The effect of water saturation on the strength of marbles. ISRM International Symposium, Tehran, Iran.

Khan, K.; M. Almarri; A. Al-Qahtani; S. Ali-Syed; A. Negara; and G. Jin (2019). Maximizing the use of rock mechanical data through empirical correlation and data-driven analytics. SPE Conference, Manama, Bahrain.

Kohmura, Y., and Y. Inada (2006). Effect of the loading rate on the stress–strain characteristics of tuff. *Journal of the Society of Materials Science*, 55: 323–328.

Li, L., and M. Aubertin (2003). A general relationship between porosity and uniaxial strength of engineering materials. *Canadian Journal of Civil Engineering*, 30(4): 644–658.

Lins, C. M. M. S.; A. Lima; and L. J. N. Guimarães (2013). Oedometer tests for evaluation of K_0 during chemical dissolution. Paper presented at the *47th U.S. Rock Mechanics/Geomechanics Symposium*, San Francisco, California.

Mihrin, D.; M. Ottaviani; M. Li; R. W. Larsen; and K. L. Feilberg (2022). Investigation of the chemical effects of long-term water flooding on reservoir rocks. *83rd EAGE Annual Conference & Exhibition*, 1–5. https://doi.org/10.3997/2214-4609.202210842.

Oluyemi, G. (2014). Conceptual physicochemical models for scale inhibitor–formation rock interaction. *Petroleum Science and Technology*, 32(3): 253–260.

Peretomode, E.; G. Oluyemi; and N. Faisal (2022). Oilfield chemical–formation interactions and their effects on petrophysical properties: A review. *Arabian Journal of Geosciences*, 15: 1223. https://doi.org/10.1007/s12517-022-10469-9.

Peretomode, E.; B. Eboibi; A. Hart; and M. Ajieh (2024). Modeling the impact of pH and reservoir temperature on the dissolution of quartz mineral due to oilfield chemical treatment. *Petroleum Science and Technology*, 1–15. https://doi.org/10.1080/10916466.2024.2412729.

Peretomode, E.; N. Faisal; and G. Oluyemi (2025). Experimental study on the effect of biocompetitive exclusion chemical on the unconfined compressive strength of sandstone reservoir rock under static saturation. *Geomechanics and Geoengineering*, 1–10. https://doi.org/10.1080/17486025.2025.2484482.

Plumb, P. A. (1994). Influence of composition and texture on failure properties of clastic rock. Eurock 94, Balkema, Rotterdam, The Netherlands.

RP40 (1998). *Recommended Practices for Core Analysis*. Society of Petroleum Engineers.

Safari, V.; G. Arzpeyma; F. Rashchi; and N. Mostoufi (2009). A shrinking particle–shrinking core model for leaching of a zinc ore containing silica. *International Journal of Mineral Processing*, 93(1): 79–83.

Sanda, O., and E. A. Taiwo (2016). Investigation of dissolution kinetics of a Nigerian columbite in hydrofluoric acid using the shrinking core model. *NIJOTECH*, 35(4): 841–846.

Shellis, R. P.; M. E. Barbour; S. B. Jones; and M. Addy (2010). Effects of pH and acid concentration on erosive dissolution of enamel, dentine and compressed hydroxyapatite. *European Journal of Oral Sciences*, 118: 475–482.

Shukla, R., et al. (2013). Mechanical behavior of rock under static saturation. *Rock Mechanics and Rock Engineering*, 46: 83–93.

Silver, G., et al. (2015). Development of a new correlation based on grain size distribution to estimate sandstone reservoir uniaxial compressive strength. International Congress of Rock Mechanics, Montreal, Canada.

Soroush, H., and B. Tokhmechi (2010). A neural network approach for real-time evaluation of sandstone strength. SPE EUROPEC/EAGE Annual Conference and Exhibition, Barcelona, Spain.

Sun, J.; L. J. Ma; M. Y. Dou; and J. Zhou (2012). Effect of strain rate on the compressive mechanical properties of concrete. *Advanced Materials Research*, 450: 244–247.

Torok, A., and B. Vasarhelyi (2010). The influence of fabric and water content on selected rock mechanical parameters of travertine: Examples from Hungary. *Engineering Geology*, 115(3): 237–345.

Vakhin, A. V. (2022). Rock mineral components' effects on heavy and shale oil transformation during aquathermolysis. *Energies*, 15(16): 6047. https://doi.org/10.3390/en15166047.

Wuyep, E.; G. Oluyemi; K. Yates; and A. Akisanya (2018). Geomechanical effects of oilfield chemicals on sand failure in reservoir rocks. *Journal of Petroleum Science and Engineering*, 165: 347–357.

Wuyep, E.; G. Oluyemi; K. Yates; and A. Akisanya (2018). Chemical and physical effects of interaction between oilfield chemicals and formation rocks and

integration with sand failure prediction models. PhD Thesis, Robert Gordon University, Aberdeen.

Wuyep, E.; G. Oluyemi; K. Yates; and A. Akisanya (2020). Evaluation of interactions between oilfield chemicals and reservoir rocks. *Natural Resources Research*, 29(2): 1239–1258.

Yang, L., et al. (2017). Fluid–rock interactions during continuous diagenesis of sandstone reservoirs and their effects on reservoir porosity. *Sedimentology*, 64(5): 1303–1321.

Yustiningtyas, L. (2012). Clay minerals in sandstone reservoir rocks: Distribution, diagenetic evolution and potential formation damage. *MTG*, 5(2).

Zheng, H.; X. Feng; and P. Pan (2015). Experimental investigation of sandstone properties under CO_2–NaCl solution–rock interactions. *International Journal of Greenhouse Gas Control*, 37.